Fine-structure splittings in high-lying ^2F states of rubidium via three-step laser spectroscopy

J. R. Brandenberger and G. S. Malyshev

Department of Physics, Lawrence University, Appleton, Wisconsin 54911, USA

Three-step laser spectroscopy has been used to measure six additional fine-structure splittings in the $n\,^2F$ states of ^{87}Rb for $11 \leqslant n \leqslant 16$. When combined with our previous measurements for $4 \leqslant n \leqslant 10$, they constitute a continuous sequence of 13 measurements suitable for comparison to fine-structure calculations in heavy alkali-metal atoms where relativistic effects, core polarization, configuration mixing, and electron correlation are important.

I. INTRODUCTION

Calculations of fine-structure (FS) splittings in heavy alkali-metal atoms require treatments of relativistic effects, core polarization, configuration mixing, and/or electron correlation going well beyond the usual central field approximations [1]. Core polarization arises from the exchange of a valence electron with electrons in the atomic core, and the spin dependence of this interaction can generate configuration mixing. Relativistic corrections as well as correlation effects stemming from the excitation of two electrons also affect fine structures especially in the low-lying levels of heavy atoms. Taken together, these interactions produce significant level shifts and even FS inversions in various alkali-metal states and elsewhere [1–4].

Dirac's expression for the FS splittings $\Delta\nu_{\mathrm{FS}}(n)$ in hydrogen can be written as $\Delta\nu_{\mathrm{FS}}(n) = \zeta(l)(1/n)^3$, where n is the principal quantum number and $\zeta(l)$ depends only on the orbital angular momentum l. This expression accounts for spin and relativistic dynamics but not for electron correlation and polarization effects. Since the latter effects are small in lighter atoms, FS splittings in the lighter alkali-metal atoms tend to satisfy the generalization $\Delta\nu_{\mathrm{FS}}(n^*) = \zeta'(l)(1/n^*)^3$, where $\zeta'(l)$ remains essentially constant for a given l, $n^* \equiv n - \delta$, and δ is the quantum defect. This expression accounts quite well for the measured FS splittings in the ^2P, ^2D, and ^2F states of the lighter alkali-metal atoms [5], but as we show in this article, it fails to predict the correct sign and correct trend in the magnitudes of the $\Delta\nu_{\mathrm{FS}}(n^*)$ for the $n\,^2F$ states of rubidium. Our experimental results confirm that the inclusion of noncentral effects such as those named previously are essential for reliable calculations of FS splittings in heavy alkali-metal atoms.

Believing that an extended series of FS measurements in a heavy alkali metal might generate theoretical interest, we continue to use three-step laser excitation to measure fine-structure splittings in the $n\,^2F_{7/2,5/2}$ states of ^{87}Rb, this time for $11 \leqslant n \leqslant 16$. By combining these results with our previous work [6], we now offer a sequence of 13 successive FS measurements.

II. EXPERIMENT

Six FS splittings in the $n\,^2F$ states of ^{87}Rb have been measured using three-step laser excitation beginning in the $5\,^2S_{1/2}(F=2) \Rightarrow 5\,^2P_{3/2}(F'=3)$ cycling transition. A saturation level of excitation of this transition at 780.03 nm

using an external-cavity diode laser [7,8] promotes a sizable rubidium population into the $5\,^2P_{3/2}(F'=3)$ state. The second step of excitation occurs at 1528.99 nm; it is also cycling and drives the $5\,^2P_{3/2}(F'=3) \Rightarrow 4\,^2D_{5/2}(F''=4)$ transition, thereby creating a significant population in the $4\,^2D_{5/2}(F''=4)$ state. This step of excitation is driven by a second external-cavity diode laser maintained on the center of the 1528.99 nm transition. The third and final step of excitation occurs at six different wavelengths: 744.617 nm for accessing the $11\,^2F$ state, 736.636 nm for the $12\,^2F$ state, 730.543 nm for the $13\,^2F$ state, 725.781 nm for the $14\,^2F$ state, 721.985 nm for the $15\,^2F$ state, and 718.904 nm for the $16\,^2F$ state. To operate at these wavelengths, we use three different diodes in a third external-cavity laser whose frequency is swept linearly in time [9].

Figure 1 summarizes the pertinent energy levels and multistep excitation scheme while Fig. 2 shows the experimental arrangement. Overlapping beams from the first two lasers counterpropagate while the third laser beam propagates parallel to the 1529-nm beam through a magnetically shielded Rb cell 20 cm in length. The first and third beams are horizontally polarized while the second is vertically polarized. Neutral density filters reduce the beam intensities to 100–500 μW/mm^2. The primary detector, a Si pin diode, monitors the transmission of the 780.03-nm pumping beam that passes through the cell. An auxiliary beam from the third laser drives an isolated Fabry-Perot interferometer so that interferograms and FS spectra can be acquired simultaneously as the third laser scans. The length of our hemispheric Fabry-Perot cavity is typically 1.5006(5) m corresponding to a free spectral range of 24.966(8) MHz.

The widths of the three-step excitation line shapes shown in Fig. 3 reflect the 6-MHz natural width (full width at half maximum) of the 780.03-nm transition augmented by as much as 10 MHz due to power broadening and the lifetimes of the other excited states. It follows that most of the rubidium atoms that participate in this three-step process fall in velocity groups that exhibit Doppler detunings of less than ± 10 MHz from the centers of the resonances. Hence the technique is nearly Doppler free.

Our $n\,^2F$ fine-structure spectra derive directly from the transmission of the 780.03-nm beam passing through the cell—not from the laser beam that actually probes the $n\,^2F$ states. This method of detection of our $n\,^2F$ resonances draws upon the fact that all three excitations are cycling [10] and therefore operate on a fixed total population distributed
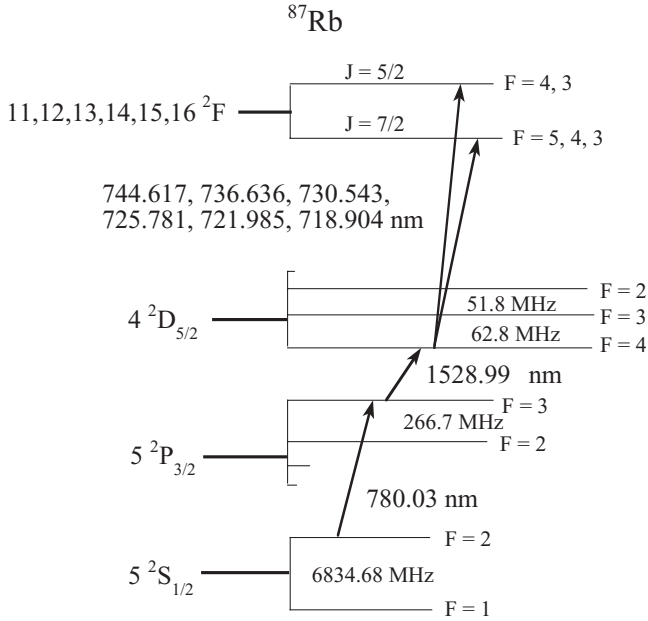
FIG. 1. Energy-level diagram showing fine and hyperfine splittings in ^{87}Rb along with the three-step excitation sequence. Note the inversion of the fine structure in the $n\,^2F$ manifolds.

among the four states. In the absence of resonances involving the $n\,^2F$ states, N_0 absorbers participate continuously in the $5\,^2S_{1/2} \Leftrightarrow 5\,^2P_{3/2}$ first-step pumping cycle (which requires about 35 ns since the $5\,^2P_{3/2}$ lifetime is 26 ns). However, in the presence of $n\,^2F$ resonances and given the comparatively long $n\,^2F$ lifetimes (about 500 ns), the $5\,^2S_{1/2}$, $5\,^2P_{3/2}$, and $4\,^2D_{5/2}$ populations suffer reductions that are also long-lived. Hence with fewer $5\,^2S_{1/2}$ atoms available to participate in the $5\,^2S_{1/2} \Leftrightarrow 5\,^2P_{3/2}$ cycling, the absorption from the 780.03-nm beam decreases. But whereas this shelving process reduces the number N_0 of $5\,^2S_{1/2} \Leftrightarrow 5\,^2P_{3/2}$ cycling atoms to $N_0(1-\delta)$, the absorption of the 780.03-nm beam falls even further since a shelved $n\,^2F$ Rb atom loses about $500/35 \approx 15$ chances to absorb and scatter the 780.03-nm beam via the $5\,^2S_{1/2} \Leftrightarrow 5\,^2P_{3/2}$ cycling. It is this "amplified" reduction in absorption that generates the increase in transmission of our 780.03-nm
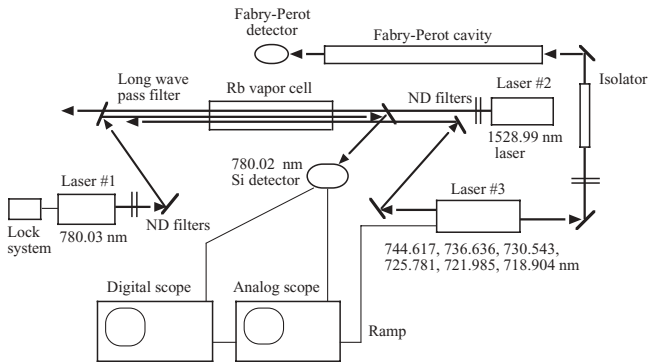

FIG. 2. Layout for three-step laser excitation spectroscopy. The ramp that sweeps laser 3 is provided by the analog scope. The digital scope captures the spectral signal riding on the 780.03-nm beam as well as the interferometric output from the Fabry-Perot detector.
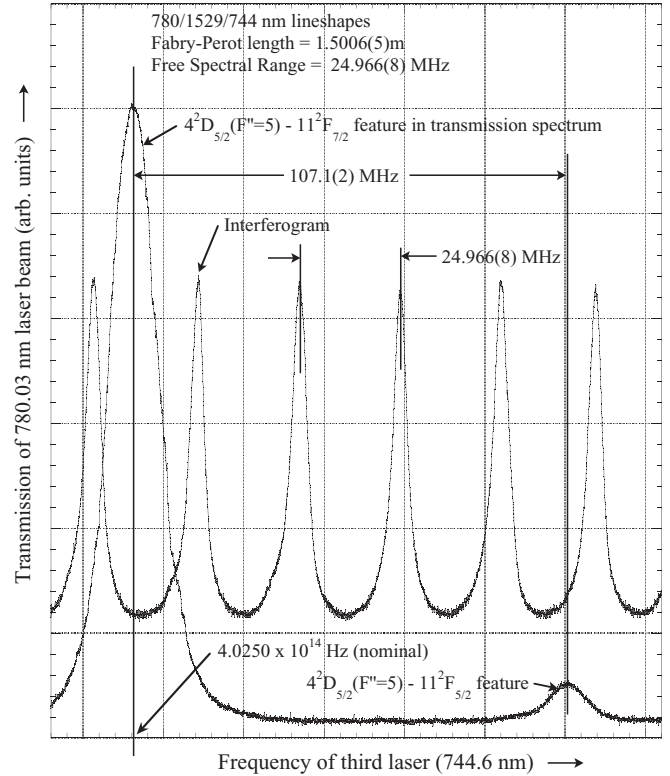

FIG. 3. Fine structure spectrum of the $11\,^2F$ state of ^{87}Rb. The transmission spectrum and interferogram are acquired simultaneously. The spectral feature on the left is located at a nominal 4.0250×10^{14} Hz. The separation between adjacent interferometric peaks is one free spectral range or 24.966(8) MHz.

beam. We have also observed these FS resonances in the transmission of the third laser beam, but the resulting signals are much weaker than our 780.03-nm signals.

III. RESULTS

Figure 3 contains a transmission spectrum pertaining to the $11\,^2F_{7/2,5/2}$ state of ^{87}Rb plotted alongside an associated Fabry-Perot interferogram that serves to calibrate the frequency scale. Digitized versions of these spectra, acquired with a dual-channel oscilloscope, consist of 5000 samplings (y_i^{spectrum}, $y_i^{\text{interferogram}}$, t_i) acquired during each 100-ms sweep, where the y_i^{spectrum} and $y_i^{\text{interferogram}}$ represent instantaneous signal voltages digitized simultaneously at successive times t_i, and where $t_{i+1} - t_i = 20\ \mu$s. Since the scanning of the third laser exhibits small frequency nonlinearities due to piezo nonlinearity and/or competition between the laser's internal- and external-cavity modes, we extract the FS splittings from the spectra by using only those segments of the interferograms that map directly onto the separations between the spectral peaks. This use of carefully chosen segments of the interferograms largely mitigates the effects of frequency nonlinearities in the scanning of the third laser since any nonlinearities in the laser scan are common to both the spectral and the interferometric traces.

TABLE I. Experimental fine-structure splittings in 13 $n\,^2F$ states of ^{87}Rb determined in this and our previous work and by other investigators.

Final state	Third-step wavelength (nm)	Fine-structure doublet	Splitting (MHz)	
			Our work	Others
$4\,^2F$	1344.28	$4\,^2F_{5/2}$–$4\,^2F_{7/2}$	−728.7(5)	−780(300)[a]
$5\,^2F$	1007.53	$5\,^2F_{5/2}$–$5\,^2F_{7/2}$	−699.5(4)	−570(300)[a]
$6\,^2F$	886.85	$6\,^2F_{5/2}$–$6\,^2F_{7/2}$	−487.1(2)	−486(4)[b]
$7\,^2F$	827.14	$7\,^2F_{5/2}$–$7\,^2F_{7/2}$	−347.1(2)	−347.6(10)[b]
$8\,^2F$	792.53	$8\,^2F_{5/2}$–$8\,^2F_{7/2}$	−250.3(2)	−150(300)[a]
$9\,^2F$	770.44	$9\,^2F_{5/2}$–$9\,^2F_{7/2}$	−184.5(3)	
$10\,^2F$	755.38	$10\,^2F_{5/2}$–$10\,^2F_{7/2}$	−138.6(2)	
$11\,^2F$	744.62	$11\,^2F_{5/2}$–$11\,^2F_{7/2}$	−107.1(2)	
$12\,^2F$	736.64	$12\,^2F_{5/2}$–$12\,^2F_{7/2}$	−84.0(3)	
$13\,^2F$	730.54	$13\,^2F_{5/2}$–$13\,^2F_{7/2}$	−67.0(2)	
$14\,^2F$	725.78	$14\,^2F_{5/2}$–$14\,^2F_{7/2}$	−54.0(3)	
$15\,^2F$	721.99	$15\,^2F_{5/2}$–$15\,^2F_{7/2}$	−44.1(2)	
$16\,^2F$	718.90	$16\,^2F_{5/2}$–$16\,^2F_{7/2}$	−36.4(2)	

[a]Ref. [11].
[b]Ref. [5].

Our FS spectra and interferograms are time averaged during acquisition. Then the FS splittings inferred from 20 such spectra are averaged to produce a final measurement. This method of double averaging produces FS determinations reliable to between 0.1% and 0.5%, uncertainties that are primarily statistical (one standard deviation of the mean). The main source of systematic uncertainty in this work stems from measuring the length of the Fabry-Perot cavity; this measurement contributes less than 0.05% uncertainty to $\Delta\nu_{FS}$.

Table I contains the results of 13 determinations of FS splittings in the $n\,^2F$ states of ^{87}Rb, the initial seven being drawn from our earlier work [6]. The negative signs reflect the observed inversions in the FS splittings (the $^2F_{7/2}$ levels always lie lower than the $^2F_{5/2}$ levels).

IV. DISCUSSION

Table I compares the FS splittings determined in this and our previous work to the measurements of others [5,6,11]. Our measurements are at least an order of magnitude more precise than those of previous investigators. Our multistep scheme, which differs from one $n\,^2F$ state to another only by the wavelength of the third laser, offers the prospect of good internal consistency from one FS measurement to the next.

As mentioned in Sec. I, hydrogenic FS splittings satisfy the expression $\Delta\nu_{FS}(n)n^3 = \zeta(l)$, where $\zeta(l)$ is constant for a given value of l. Figure 4 compares the products $\Delta\nu_{FS}(n)n^3$ for three hydrogenic cases (where the values of $\zeta(l)$ are calculated using Dirac's expression) to the corresponding product $\Delta\nu_{FS}(n^*)(n^*)^3$ applicable to the $n\,^2F$ splittings measured in our work. The comparison is quite revealing: (1) the product $\Delta\nu_{FS}(n^*)(n^*)^3$ plotted as a function of n^* is smoothly decreasing and negative in contrast to the constant and positive hydrogenic values; (2) surprisingly, the plot of $\Delta\nu_{FS}(n^*)(n^*)^3$ versus n^* closely resembles a simple decaying exponential

(see the dashed line in Fig. 4); (3) the signs of all the $\Delta\nu_{FS}$ for Rb are negative in agreement with the established pattern that fine structures in the low-lying $n\,^2F$ states of Rb are always inverted; (4) there is no indication that the values of $\Delta\nu_{FS}(n^*)$ for Rb are likely to change sign for larger values of n^*; and (5) the absolute magnitudes of the products $\Delta\nu_{FS}(n^*)(n^*)^3$ for the $n\,^2F$ states of Rb are substantially larger than those of their $n\,^2F$ hydrogenic counterparts.

Several authors [1–4] have invoked relativistic effects, core polarization, correlation treatments, and/or configuration mixing to calculate FS splittings in both light and heavy
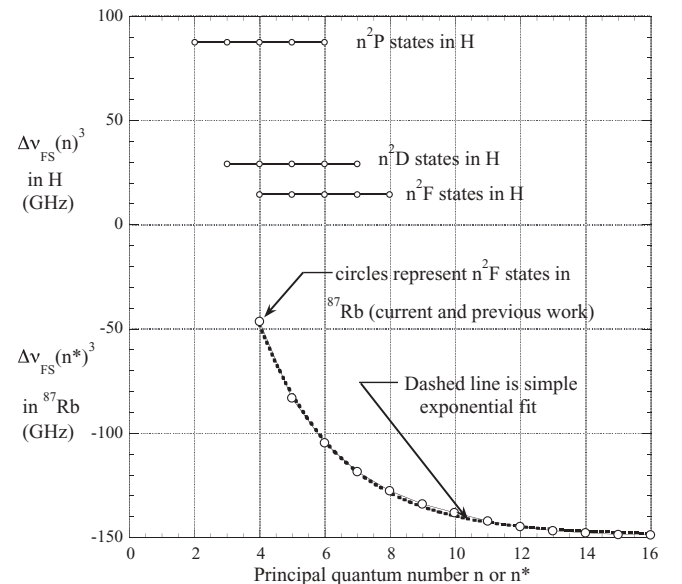

FIG. 4. Trends in products $\Delta\nu_{FS}(n)^3$ versus n for ^2P, ^2D, and ^2F states of H and contrasting trend in product $\Delta\nu_{FS}(n^*)^3$ versus n^* for n^2F states of ^{87}Rb.

alkali-metal atoms. Some of these attempts have accounted successfully for the inversion of the fine structures, but to date no one has attempted detailed calculations of the fine structures of the $n\,^2F$ states of rubidium. Any further investigation of this situation must await new efforts to calculate these FS splittings.

[1] I. Lindgren and Ann-Marie Mårtensson, Phys. Rev. A **26**, 3249 (1982).

[2] E. Luc-Koenig, Phys. Rev. A **13**, 2114 (1976); J. Phys. (Paris) **41**, 1273 (1980).

[3] T. Lee, J. E. Rodgers, T. P. Das, and R. M. Sternheimer, Phys. Rev. A **14**, 51 (1976); R. M. Sternheimer, J. E. Rodgers, T. Lee, and T. P. Das, *ibid*. **14**, 1595 (1976).

[4] N. C. Pyper and P. Marketos, J. Phys. B **14**, 4469 (1981).

[5] J. W. Farley and R. Gupta, Phys. Rev. A **15**, 1952 (1977).

[6] J. R. Brandenberger, C. A. Regal, R. O. Jung, and M. C. Yakes, Phys. Rev. A **65**, 042510 (2002).

[7] All wavelengths quoted in this paper are measured in air.

[8] This external-cavity laser, which reflects our own design, is locked to the $5\,^2S_{1/2}(F=2) \Rightarrow 5\,^2P_{3/2}(F'=3)$ transition using the DAVLL technique described in V. V. Yashchuk *et al.*, Rev. Sci. Instrum. **71**, 341 (2000); K. L. Corwin *et al.*, Appl. Opt. **37**, 3295 (1998).

[9] The single-mode, 20- to 50-mW diodes employed in these external-cavity lasers are supplied by Frankfurt Laser, Optima Precision, Thorlabs, and Power Technology.

[10] Strictly speaking, the $4\,^2D_{5/2}$–$n\,^2F_{7/2}$ third step transition and; the weaker $4\,^2D_{5/2}$–$n\,^2F_{5/2}$ transition are not perfectly cycling, but their spontaneous branching to other lower states are weak.

[11] I. Johansson, Ark. Fys. **20**, 135 (1961).